Archives of Civil and Mechanical Engineering (2022) 22:121
https://doi.org/10.1007/s43452-022-00444-2

ORIGINAL ARTICLE

Synthesis and characterization of alkali-activated materials containing biomass fly ash and metakaolin: effect of the soluble salt content of the residue

S. Jurado-Contreras[1] · E. Bonet-Martínez[1] · P. J. Sánchez-Soto[2] · O. Gencel[3] · D. Eliche-Quesada[1,4]

Received: 22 January 2022 / Revised: 21 March 2022 / Accepted: 12 April 2022

Abstract
The present study investigates the production and characterization of alkali-activated bricks prepared with mixing metakaolin (MK) and biomass fly ash from the combustion of a mix of pine pruning, forest residues and energy crops (BFA). To use this low cost and high availability waste, different specimens were prepared by mixing MK with different proportions of BFA (25, 50 and 75 wt%). Specimens containing only metakaolin and biomass fly ash were produced for the purpose of comparison. Effects of the alkali content of biomass fly ash, after a washing pretreatment (WBFA), as well as the concentration of NaOH solution on the physical, mechanical and microstructural properties of the alkali-activated bricks were studied. It was observed that up to 50 wt% addition of the residue increases compressive strength of alkali-activated bricks. Alkalinity and soluble salts in fly ash have a positive effect, leading materials with the improved mechanical properties. Concentration of NaOH 8 M or higher is required to obtain optimum mechanical properties. The compressive strength increases from 23.0 MPa for the control bricks to 44.0 and 37.2 MPa with the addition of 50 wt% BFA and WBFA, respectively, indicating an increase of more than 60%. Therefore, the use of biomass fly ash provides additional alkali (K) sources that could improve the dissolution of MK resulting in high polycondensation. However, to obtain optimum mechanical properties, the amount of BFA cannot be above 50 wt%.

Keywords Biomass fly ash · Metakaolin · Alkali-activated bricks · Mechanical properties

1 Introduction

Ordinary Portland cement (OPC) is the most widely used hydraulic binder in the world. Despite its innumerable advantages (relatively low cost, easy availability of raw materials very abundant in the earth's crust, acceptable durability), it is, however, a highly polluting manufacturing material, as it requires a large amount of electrical and thermal energy (temperatures above 1400–1500 °C need to be reached), exploits natural resources (obtaining raw materials causes the destruction of natural quarries) and emits a large amount of polluting gases into the atmosphere. These gases cause the greenhouse effect (CO_2, SO_2, NO_X). Environmental regulations oblige the cement industry and the scientific community to seek solutions to achieve the goal of sustainable development. This is reached through process efficiency or the development of new, more eco-efficient binder materials.

These eco-efficient cements are defined as those binders that are obtained through processes that require less energy than OPC and also have a lower environmental impact. Among the alternative cements developed are cements with additions in which the partial replacement of OPC by the incorporation of chemically active additions such as pozzolans and industrial by-products such as coal ash and steel slag has been achieved. Hasmi et al. [1, 2] indicated that the

✉ D. Eliche-Quesada
deliche@ujaen.es

1 Department of Chemical, Environmental and Materials Engineering, Higher Polytechnic School of Jaén, University of Jaén, Campus Las Lagunillas, 23071 Jaén, Spain

2 Institute of Materials Science of Sevilla (ICMS), Joint Center of the Spanish National Research Council (CSIC), University of Sevilla, 41092 Seville, Spain

3 Civil Engineering Department, Bartin. University, Bartin, Turkey

4 Center for Advanced Studies in Earth Sciences, Energy and Environment (CEACTEMA), University of Jaén, Campus Las Lagunillas s/n, 23071 Jaén, Spain

Published online: 07 May 2022

use of fly ash in concrete improves the mechanical properties due to its pozzolanic behaviour. The creep and fracture state of reinforced concrete with up to 40 wt% fly ash shows a trend identical to that of reinforced concrete without fly ash. Furthermore, concrete with 40 wt% fly ash showed a satisfactory behaviour at older ages (i.e. beyond 28 days) in terms of strength, modulus of elasticity and deflection. Among these eco-efficient cements there are also others with very different characteristics from OPCs, the so-called Alkali-activated Materials (AAMs), which are defined as binders resulting from the chemical interaction of strongly alkaline solutions and aluminosilicates of different compositions (high and low CaO content) and natural origin such as metakaolin, produced from the calcination of kaolinite clays as well as other calcined clays [3] or industrial wastes and by-products such as blast furnace slag, fly ash, ceramic residues [4, 5].

Alkaline cements are materials obtained by a chemical process or alkaline activation of a material based on aluminosilicates. These materials are rich in alumina (Al_2O_3) and silica (SiO_2), with totally or partially amorphous structure, acting as initiators of the reaction with an alkaline activator [6, 7]. Aluminosilicates susceptible to alkaline activation can be divided into two groups according to their chemical composition: (i) calcium-rich materials, belonging to the system (Na, $K)_2O$–CaO–Al_2O_3–SiO_2–H_2O and (ii) calcium-poor materials, belonging to the system (Na, $K)_2O$–Al_2O_3–SiO_2–H_2O [8]. Therefore, when these materials react, two phases can be produced: sodium aluminosilicate gel hydrate (NASH) and calcium silicate hydrate (CSH). These two networks act differently. The NASH network produces a three-dimensional structure, while the CSH network resembles that of a polymer [9].

The level of interest in alkaline activated materials, has increased in recent years due to their high mechanical properties and durability in terms of chemical and fire resistance [5] in addition to the environmental benefits they bring [10], reducing CO_2 emissions because their production does not require high temperatures [11].

Andalusia has an important biomass wealth, largely from olive cultivation and its derived industries. It can be considered that one hectare of olive grove can produce 2–3 tons of prunings [12]. The energy use of pruning has traditionally been linked to the use of firewood as domestic fuel; however, during the last decade, the use of olive pruning chips as fuel for electricity generation has experienced a significant increase. At present, this consumption is almost exclusively linked to biomass electricity generation plants. In areas where there is no possibility to sell the biomass, burning and feeding it into the soil remain the farmer's only options. In Andalusia, the use of forest biomass has great potential. The need to carry out silvicultural treatments for the maintenance and improvement of forests and forest masses through felling, pruning, clearing of bushes, etc. generates residues (firewood, branches and bushes) that must be removed from the forest, as they are a risk factor of serious importance for the spread of pests and forest fires. These residues can be used in the energy field. Energy crops are specific crops dedicated exclusively to energy production. Numerous public and private experiences have been carried out in Andalusia for the testing and production of different herbaceous and tree species for energy purposes, in which traditional food crops, such as cereals, sunflower, rapeseed, with a suitable aptitude for the production of biofuels, as well as herbaceous and forest species for obtaining solid biomass for thermal and/or electrical use, have been evaluated.

Biomass ash is the solid residue from biomass combustion. Nowadays, the use of biomass to generate heat and electricity, to apply waste and reduce CO_2 emissions to the atmosphere, has increased substantially and has become the fastest growing renewable energy. Consequently, the amount of ash available is also growing. The ash produced by the combustion process is of two types; bottom ash and fly ash. Bottom ash is produced on the grate and in the combustion chamber and consists of fully or partially burned biomass, while fly ash is entrained in the combustion gases that are collected and precipitated in the filters. The fields of application of biomass ashes depend on their characteristics, such as chemical composition, morphology, mineralogical composition and leaching behavior. The alternatives of the produced ashes contemplate their transfer to authorized landfills, with the expense and space occupation that it entails being the less attractive alternative. Other more sustainable alternatives are its use as fertilizer [13], its applications in construction as raw material in the manufacture of cements, concretes, ceramic products, filler in road embankments [14–19], nanotechnology in industrial catalysis and environmental [19] and its reuse as fuel [20].

Other authors reported the use of different biomass fly ashes in the manufacture of alkaline activated materials. Thus, Laxman Yadav et al. [21] studied the effect of compressive strength of various parameters, such as silica/alumina ratio, the effect of alkaline activator/binder ratio and the effect of sodium silicate/sodium hydroxide ratio in sugarcane bagasse-metakaolin ash mortars. Optimum results were obtained for a silica/alumina ratio 2.5 (56.36 wt% bagasse fly ash-43.64 wt% metakaolin), an activator/alkaline binder ratio of 0.5 and a sodium silicate/sodium hydroxide ratio of 2.5. Nana et al. [22] studied the effect of replacing metakaolin with volcanic ash, VA (10–30 wt%) and rice husk ash, RHA (0–20 wt%) in the manufacture of geopolymers. The results showed that the mechanical strengths and physical properties were mainly affected by VA content as well as RHA content, where the optimum mechanical strengths were obtained for specimens containing 20 wt% VA and 10 wt% RHA. De Rossi et al. [23] studied the influence of processing

parameters on the properties of geopolymers based on wood biomass fly ash. The results showed different physical and chemical properties as a function of processing parameters, suggesting various applications. Samples obtained under ambient conditions with a sodium silicate: sodium hydroxide (SS: SH) = 1.5 ratio could be used as dense mortars. Perná et al. [24] studied the addition of 20 and 33 wt% of high LOI straw ash as filler in metakaolin-based geopolymers investigating the quality of its incorporation and its influence on the resulting properties. Yurt and Bekar [25] have studied the effect of using hazelnut shell ash (HA) together with metakaolin and blast furnace slag (BFS) in the production of alkaline activated concrete. They concluded that ashes can be effectively used in alkaline activated concrete mixtures and have potential to improve the abrasion resistance of the materials. Rajamma et al. [26] studied the effect of addition of metakaolin to biomass fly ash in the manufacture of alkaline activation mortars. It is concluded that addition of up to 40 wt% metakaolin results in specimens with the improved mechanical properties.

The aim of this work is to evaluate the use of biomass fly ash from a mix of olive pruning, forestry residues and energy crops as a raw material to replace metakaolin (MK) in the manufacture of alkaline activated cements. The effect on the technological properties of the alkaline activation cements of the amount of residue to be replaced by MK has been studied. Furthermore, the alkalinity and content of soluble salts in the residue, subjecting it to a washing pre-treatment, and the concentration of the NaOH solution used have been also studied.

2 Experimental procedure

2.1 Raw materials

The raw materials used for the synthesis of alkali-activated bricks were: a natural kaolin (provide by Caobar S.A. Póveda de la Sierra, Guadalaja, Spain), received as a powder product and calcined at 750 °C (4 h) in an electric furnace Carbolite to transform into the reactive metakaolin phase [27–29]. The biomass fly ash (Aldebarán Energía del Guadalquivir, Andújar, Jaén, Spain) obtained from the combustion of a mix of olive pruning, forest residues and energy crops. To observe the effect of alkalinity and the content of soluble salts in the mechanical properties of the bricks, the fly ashes were used as they were received from the renewable energy generation plant and subjected to a pretreatment process. The pretreatment consists in a washing and drying process. A 1:3 (wt/wt) ash/water ratio was shaked in a beaker at 60 °C for 1 h. The ash suspension was filtered with a nitrocellulose filter and dried at 110 °C up to constant weight. The particle size of ash (BFA), washed ash (WBFA) and metakaolin used as raw material was determined the particle size distibution by laser diffraction (Fig. 1) using a Malvern Mastersizer 2000 equipment and the d_{10}, d_{50} and d_{90} values are presented in Table 1. Table 1 shows that metakaolin is a finer material than fly ash. However, most of the particles of both raw materials are smaller than 150 microns, so it is expected a good chemical reactivity of them with the alkaline solution.

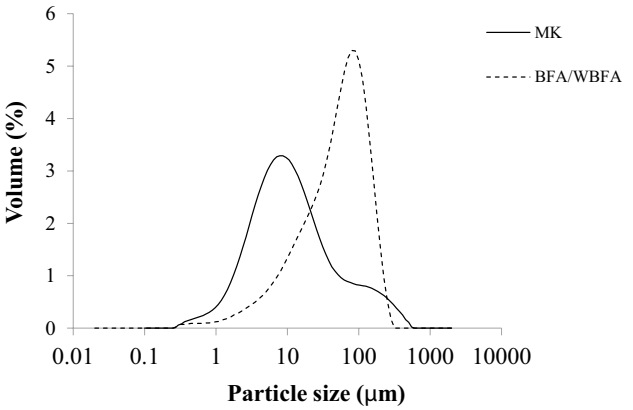

Fig. 1 Particle size distribution of raw materials

Table 1 Particle size of ashes (BFA), washed ashes (WBFA) and metakaolin (MK)

Precursors	d_{10} (μm)	d_{50} (μm)	d_{90} (μm)
BFA/WBFA	8.06	51.97	133.92
MK	2.23	9.58	87.02

The chemical composition of the precursors was analyzed by X-ray fluorescence (XRF) (Philips Magix Pro model PW-2440). Approximately 0.8 g of sample and 8 g of flux (mixture of LiB_4O_7 66.67%, $LiBO_2$ 32.83%, LiBr 0.5%) were mixed. Subsequently, a bead was made by melting using a bead machine (model Katanax X600 from Spex Sample Prep). The samples were analysed under vacuum. Concentration data were obtained using the integrated UNIQUANT software, in the form of oxides, using an overall Kappa (bead) corrected with different CRMs and taking into account the percentage of loss of ignition (LOI). The results are shown in Table 2. The washing pretreatment reduced the potassium content of the ashes from ~ 8.0% to 1.84%. The total $SiO_2 + Al_2O_3 + Fe_2O_3$ value is 32.4% and 36.0% for BFA and WBFA, respectively. The CaO value is 34.54% and 38.15% for BFA and WBFA, respectively. The CaO content has an influence over the mechanical properties of the alkali-activated materials due to the additional $CaO–Al_2O_3–SiO_2–H_2O$ (C–A–S–H) phases [30, 31] generated during the geopolymerization of $Na_2O–Al_2O_3–SiO_2–H_2O$ (N–A–S–H). These ashes classified as "C" class fly ash [32] rich in carbonates, oxyhydroxides

Table 2 Chemical composition (main oxide content wt%), LOI (loss of ignition) and true density of precursors: MK, BFA and WBFA

Component (wt%)	MK	BFA	WBFA
SiO_2	58.03	22.08	24.54
Al_2O_3	40.29	6.65	7.69
Fe_2O_3	0.42	3.64	3.81
MnO	–	0.16	0.19
MgO	–	4.77	5.30
CaO	0.11	34.54	38.15
Na_2O	0.09	1.91	0.93
K_2O	0.02	7.99	1.84
TiO_2	0.15	0.65	0.59
P_2O_5	0.07	2.33	2.62
SO_3	0.01	5.27	2.55
LOI	0.36	9.99	10.29
True density (kg/m^3)	2631	2553	2431

silicates, and some sulphates and phosphates. The silica/alumina (SiO_2/Al_2O_3) ratio is 3.32 and 3.19 for BFA and WBFA, respectively.

The mineralogical composition of the metakaolin and the residues BFA and WBFA and alkali-activated materials were determined by X-ray diffraction (XRD) (Empyrean equipment with a PIXcel-3D detector from PANalytical) the 2θ range from 10 to 60 with a step size of 0.02 (Fig. 2). The phases in XRD were determined in Highscore software. MK consisted of quartz (file card number: 96-900-5020) as the only crystalline phase. The broad hump structures observed from 15° to 35° (2θ), corresponds to the presence of amorphous phase associated to metakaolin. The BFA residue consists mainly of quartz (96-900-5020) as the predominant mineral, calcite (file card number: 96-900-9669) and to a lesser extent aluminosilicates (file card number: 96-900-1967) and sylvite (file card number: 96-900-3130). After the washing process, the diffraction patterns of the WBFA show an increase in the carbonate content of the ashes, and the diffraction peaks corresponding to sylvite is not observed. The presence of amorphous phase in the residue can be observed by the deviation of the baseline in the 2θ region between 20° and 35°.

The different chemical bonds of the precursors and alkali-activated bricks were investigated by Attenuated Total Reflectance-Fourier Transform Infrared spectroscopy ATR-FTIR (Vertex 70 Bruker equipment). The scans recorded in frequency range 4000–400 cm^{-1}. Figure 3 shows the FTIR spectra of the precursors: MK, BFA and WBFA. The band centered at 1058 cm^{-1} in the MK precursor and the centered bands appearing at frequencies 960–1150 cm^{-1} in the BFA and WBFA waste materials are pointed to the asymmetric stretching vibration of the Si–O–T (Si, Al) bond [33, 34]. They are indicative of the presence of silicon oxide in the samples. In the samples of the BFA residue and subjected

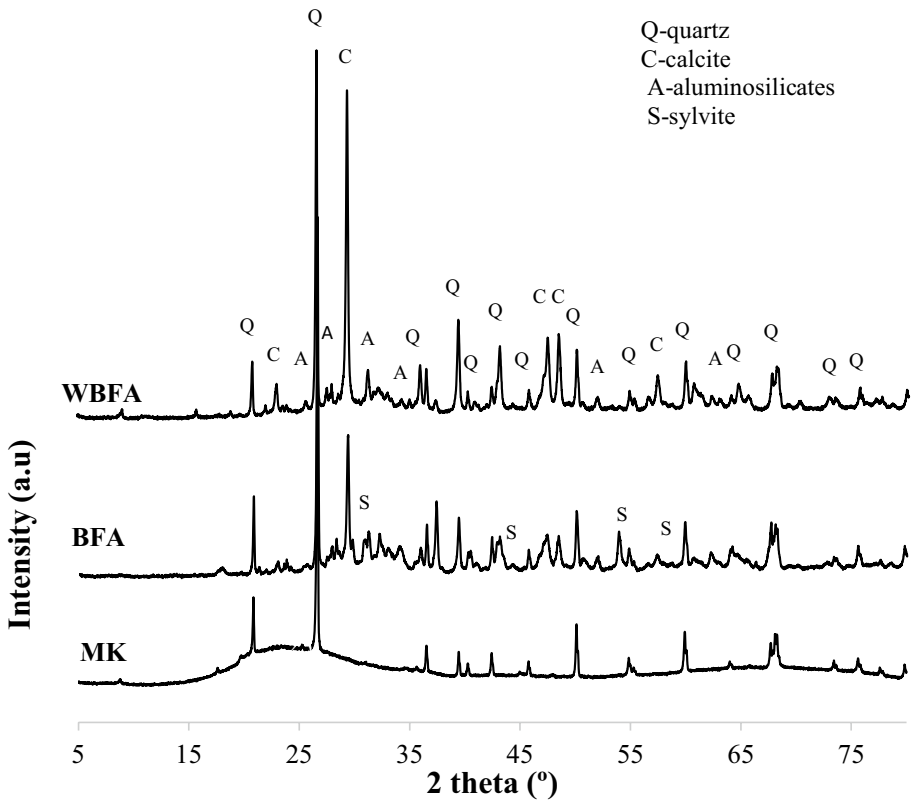

Fig. 2 XRD pattens of BFA, WBFA and MK

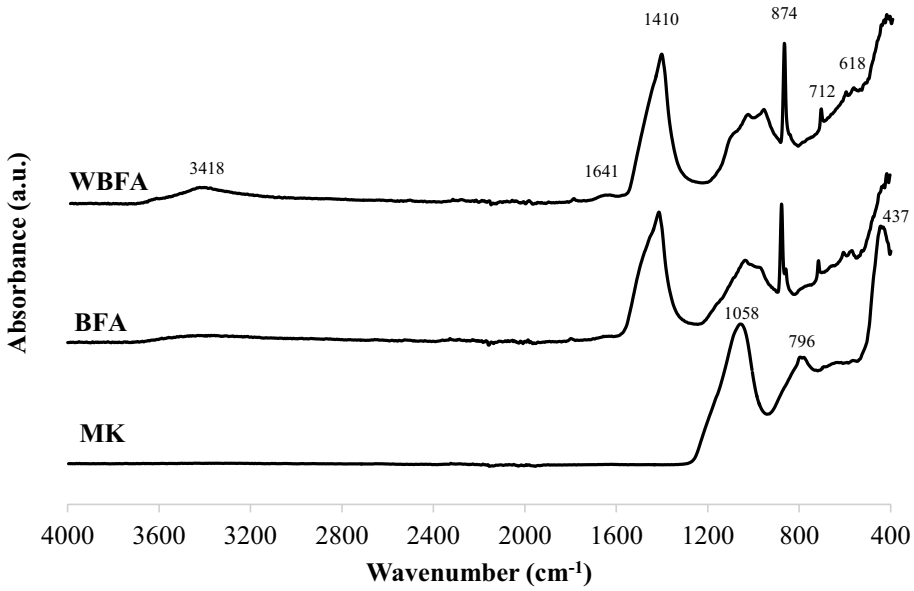

Fig. 3 FTIR spectra of raw materials: MK, BFA and WBFA

to the wash pretreatment, WBFA, several peaks corresponding to the different symmetries of the $[SiO_4]^{4+}$ group are distinguished [35]. The washing pretreatment has decreased the stretching of the silicon bonds, revealing that the pozzolanic reactivity of ashes decreased. In the MK precursor the band at 796 cm^{-1} corresponds to the Si–OSi–O–Si bond vibration of quartz [36] and the band centered at 437 cm^{-1} is assigned to the bending or stretching vibration of T–O–T bridges (T = Si or Al) of aluminosilicates [37]. In the residue without and with pretreatment, high absorption bands at 1410 cm^{-1} along with a narrow peak at 874 cm^{-1} and a weak absorption at 712 cm^{-1} are observed, associated with C–O bond vibrations in carbonate $[CO_3]^{2-}$ groups. In addition to a weak band at 618–603 cm^{-1} assigned to Si–O bond vibration.

In ashes, after washing pretreatment, a broad band centered at 3418 cm^{-1} and a shoulder centered at 1641 cm^{-1} corresponding to O–H bond tension and O–H–O bond bending in water, respectively, were identified [38].

The morphology of the MK precursor and residue without pretreatment and after washing pretreatment was observed by a JEOL SM 840 field emission scanning electron microscope (SEM) and the chemical composition was determined by energy dispersive X-ray spectroscopy (EDS). Microstructure of fractured surfaces were examined using SEM. Samples were placed on an aluminum sample holder and coated with carbon using the JEOL JFC 1100 sputter coater. The SEM images and EDS spectra obtained of raw materials are shown in Fig. 4.

As can be seen, the MK precursor has irregularly shaped particles with an irregular particle size distribution. Most of them are rich in silica and alumina (Spectrum 1) and in smaller proportion presents particles rich in silica (Spectrum 2). The BFA and WBFA residue, presents some spheres and more spherical particles being rich in silica and alumina in addition to calcium. The amount of potassium in the particles after the washing pretreatment is slightly lower. In addition, BFA and WBFA presented particles rich in calcium (Spectrum 4). After the washing pretreatment, no particles other than those rich in silica and alumina, rich in potassium, are observed (Spectrum 5).

Leachates from fly biomass ash were characterized by ICP-MS according to methods adapted from UNE-EN ISO 17294–1:2007 [39] and UNE-EN ISO 17294-2:2017 [40] (Table 3). The leachate is alkaline (pH = 13), due to soluble salts, mainly potassium hydroxide and carbonate, as well as sulfates and chlorides. Therefore, this leachate provides an elevated pH that could favor geopolymerization reactions. The dry matter was 36.5 g/l, potassium representing 10.6 g/l. The conductivity is 68,000 µS/cm. It is, therefore, interesting to study the beneficial effect of these soluble salts in the manufacture of alkali-activated bricks.

2.2 Sample preparation and characterization

The activating solution contains sodium hydroxide (Panreac SA, purity of 98%) and sodium silicate (Panreac S.A.) with a weight composition: 29.2% SiO_2, 8.9% Na_2O and 61.9% H_2O. The alkaline activator solutions were prepared in two main stages. In the first stage, the sodium hydroxide solution of the appropriate molarity is prepared to which, once cooled, the appropriate amount of sodium silicate is added. In the first stage of the study, when the influence of the BFA or WBFA content on the addition of MK is studied, the molarity of the sodium hydroxide solution is 8 M and the sodium silicate/sodium hydroxide ratio = 1.15 being the

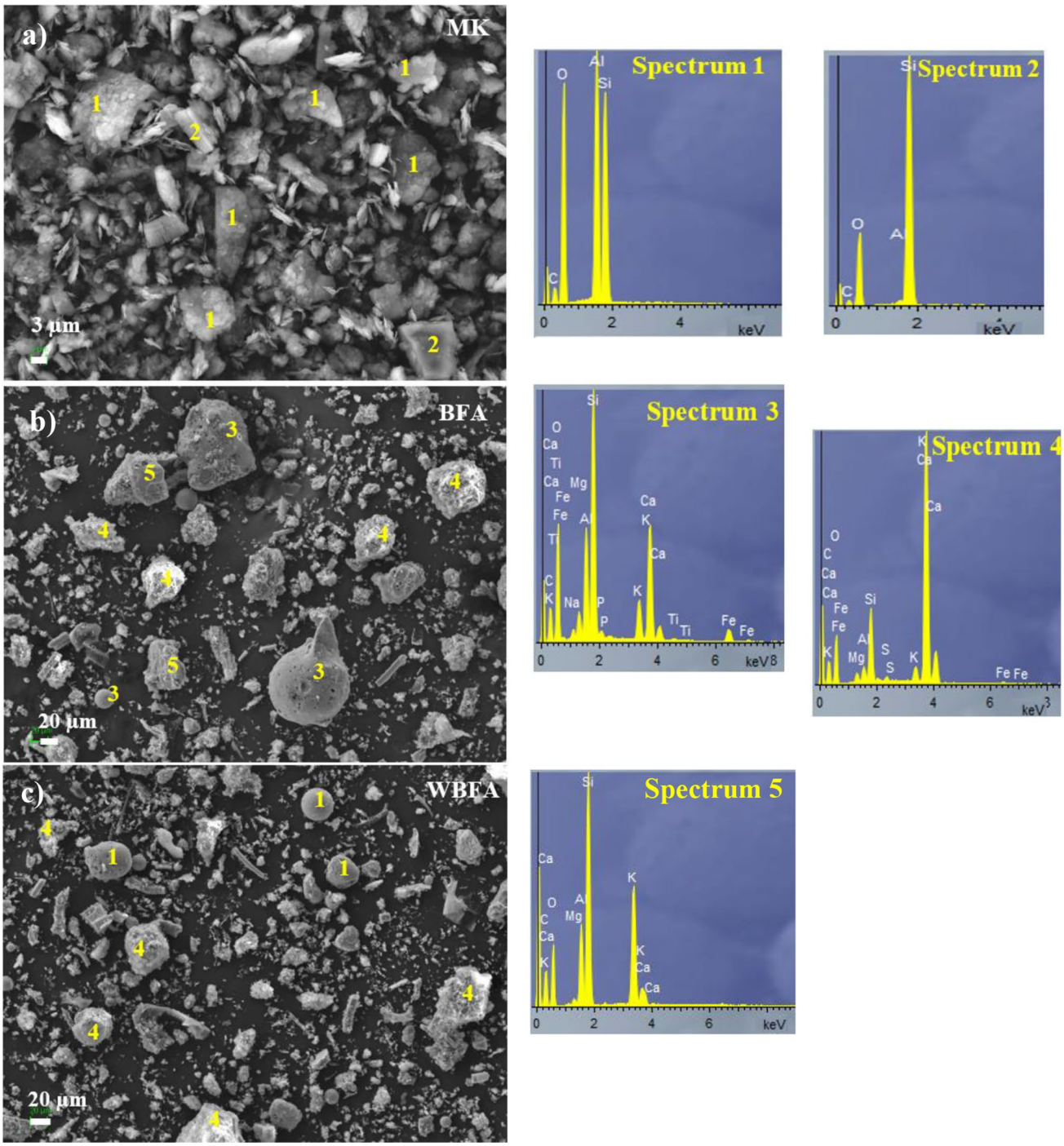

Fig. 4 SEM images and EDS spectra of raw materials: **a** MK, **b** BFA and **c** WBFA

modulus of the activator ($Ms = SiO_2/Na_2O = 1.2$). Once the amount of BFA and WBFA to be substituted by the MK has been optimized, the influence of the concentration of the NaOH solution (5, 8, 12 M) was studied.

In the preparation of alkali-activated bricks, solid precursors obtained by mixing metakaolin are replaced by 25–100 wt% of BFA or WBFA. The mixture of solid precursors was mixed with the activating solution. The details of the different formulations are presented in Table 4. For each formulation in which the effect of the addition of BFA or WBFA is studied, the water/binder ratio was kept constant at 0.6 obtaining an acceptable workability. The activator was added to the precursors previously mixed for 2 min and the mixture agitated for

Table 3 Physico-chemical characteristics of leachate from washing of fly biomass ash

Property	Leachate
pH	13
Electrical conductivity (μS/cm)	68,000
Dry matter (180 °C) (mg/l)	36,500
Sodium (mg/l)	337.5
Potassium (mg/l)	10,593.1
Calcium (mg/l)	870.35
Magnesium (mg/l)	0.0571
Iron (mg/l)	0.046
Manganese (mg/l)	0.0005
Chloride (mg/l)	675.2
Sulphur (mg/l)	2783.9

approximately 5 min in a Proeti planetary mixer. The fresh paste obtained was poured into silicone molds (60 × 30 × 15 mm) and vibrated for 2 min to avoid air bubbles. The samples were cured at 60 °C (24 h and humidity saturated atmosphere), demolded and kept at room temperature until the test day (28 days) (Fig. 5). The alkali-activated bricks obtained are shown in Fig. 6. The parameters of this study were the amount of BFA to be added to MK, the influence of soluble salts in the ashes, i.e., of the ash pretreatment, and the modulus of the activator. These parameters are used to optimize the compressive strength of alkali-activated bricks.

The bulk density and apparent porosity of the bricks were determined according to the UNE-EN 1015-10 standard [41]. These parameters evaluated by triple weighing of the alkali-activated samples after water saturation, suspended in distilled water and after drying at 80 °C, until constant weighing. Water absorption analysis was carried out according to ASTM C-642 [42].

The compressive strength of six geopolymer bricks for each composition was performed using a universal testing machine MTS 810 Material Testing Systems Laboratory of 100 kN with a displacement of 0.5 mm/min according to UNE-EN-772–1 [43].

3 Results and discussion

3.1 Bulk density, apparent porosity and water absorption

Figure 7 shows the bulk density, apparent porosity and water absorption values of the alkali-activated bricks after 28 days of curing. As can be seen, the bulk density increases as the substitution ratios of metakaolin for BFA residue increase. The water absorption and apparent porosity values are in agreement with bulk density results. Alkali-activated bricks with lower bulk density had higher water absorption and bulk porosity and vice versa. The control bricks have a bulk density of 1250 kg/m^3, apparent porosity of 38% and a water absorption of 34%. Substitution of MK by BFA results in bricks with higher bulk densities in the range of 1277–1625 kg/m^3, apparent porosity in the range 38–18% and water absorption in the range 33–12%, lower as increasing amounts of BFA residue incorporated. The real density measured with He of MK (2631 g/cm^3) is higher than that of BFA (2553 kg/m^3) (Table 2), indicating a lower particle mass to volume ratio when the weight percentage of BFA was increased. Therefore, the increase in bulk density and decrease in porosity may be due to a lower fluidity of the obtained pastes as increasing amounts of ash are

Table 4 Alkali-activated bricks mix proportion of considered parameters

AAM	MK (g)	BFA (g)	WBFA (g)	NaOH (g)	H_2O (g)	Na_2SiO_3 (g)	*w/b*	Ms	Molar ratio		
									Si/Al	Na/Si	Ca/Si
100MK	450	–	–	64	195	300	0.6	1.2	1.63	0.42	0.002
75MK-25BFA	337.5	112.5	–	64	195	300	0.6	1.2	1.83	0.48	0.14
50MK-50BFA	225	225	–	64	195	300	0.6	1.2	2.15	0.56	0.31
25MK-75BFA	112.5	337.5	–	64	195	300	0.6	1.2	2.85	0.67	0.54
100BFA	–	450	–	64	195	300	0.6	1.2	5.31	0.82	0.89
75MK-25WBFA	337.5	–	112.5	64	195	300	0.6	1.2	1.83	0.48	0.15
50MK-50WBFA	225	–	225	64	195	300	0.6	1.2	2.15	0.55	0.34
25MK-75WBFA	112.5	–	337.5	64	195	300	0.6	1.2	2.81	0.64	0.59
100WBFA	–	–	450	64	195	300	0.6	1.2	4.86	0.78	0.93
50MK-50BFA	225	225	–	40	195	300	0.6	1.6	2.15	0.43	0.31
50MK-50BFA	225	225	–	96	195	300	0.58	0.9	2.15	0.73	0.31
50MK-50WBFA	225	–	225	40	195	300	0.63	1.6	2.15	0.42	0.34
50MK-50WBFA	225	–	225	96	195	300	0.58	0.9	2.15	0.72	0.34

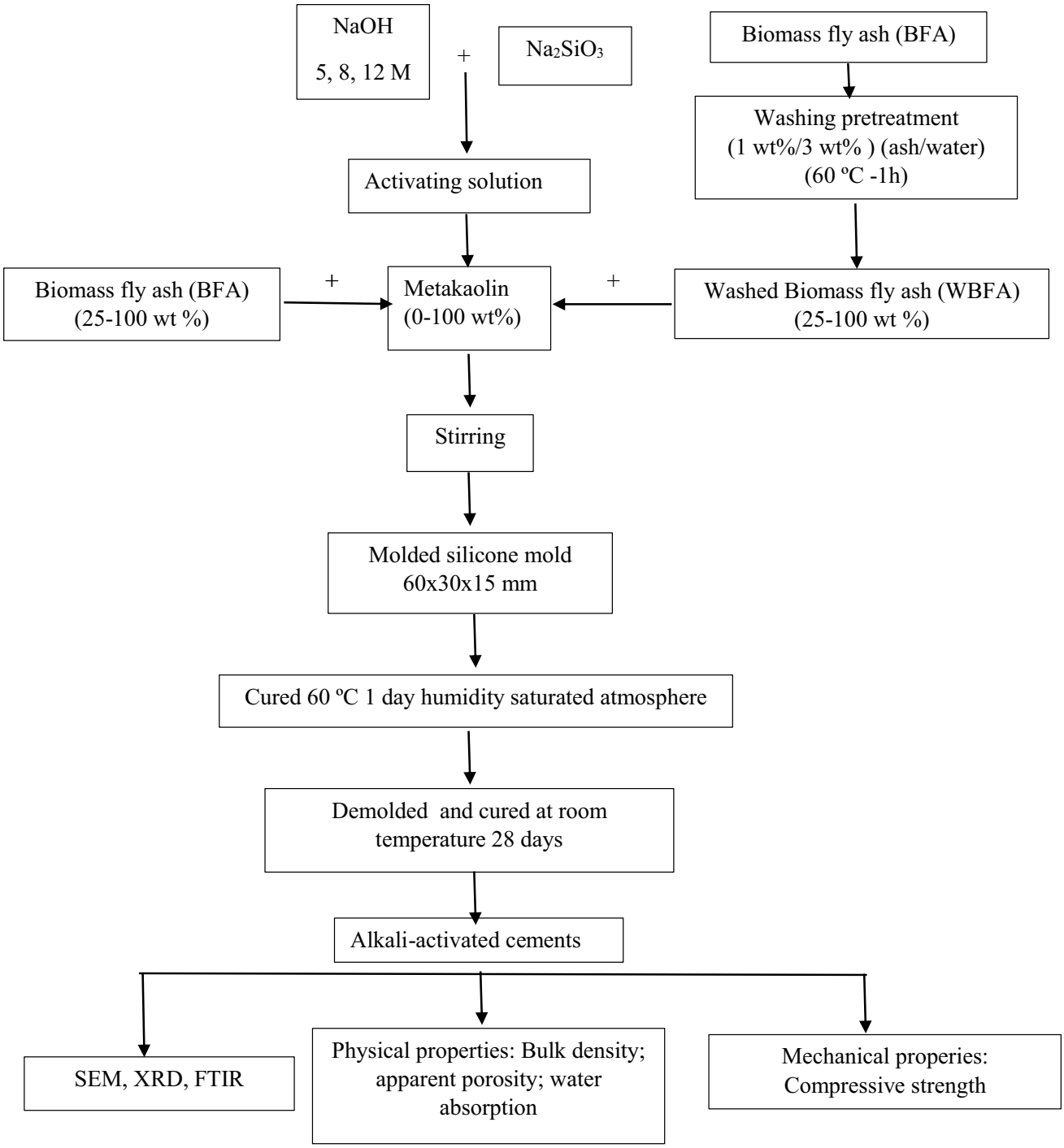

Fig. 5 Synthesis and characterization scheme of alkali-activated cements

incorporated, which could improve the formation of a more compact and dense structure of the samples with the addition of BFA. The residue served as a filler with a good ability to fill spaces, voids and pores.

In the case of the influence of the washing pretreatment, it was noted that alkali-activated bricks with slightly lower bulk densities, with values in the range of 1254–1545 kg/m^3 are obtained. On the other hand, values of apparent porosity between 38% and 21% and water absorption between 35% and 14%, slightly higher, are obtained. The lower bulk density for the same amount of residue incorporated after the washing process may be due to the lower real density of the ashes after pretreatment, decreasing to 2431 kg/m^3 (Table 2), which

Fig. 6 Alkali-activated bricks prepared as described in experimental procedure

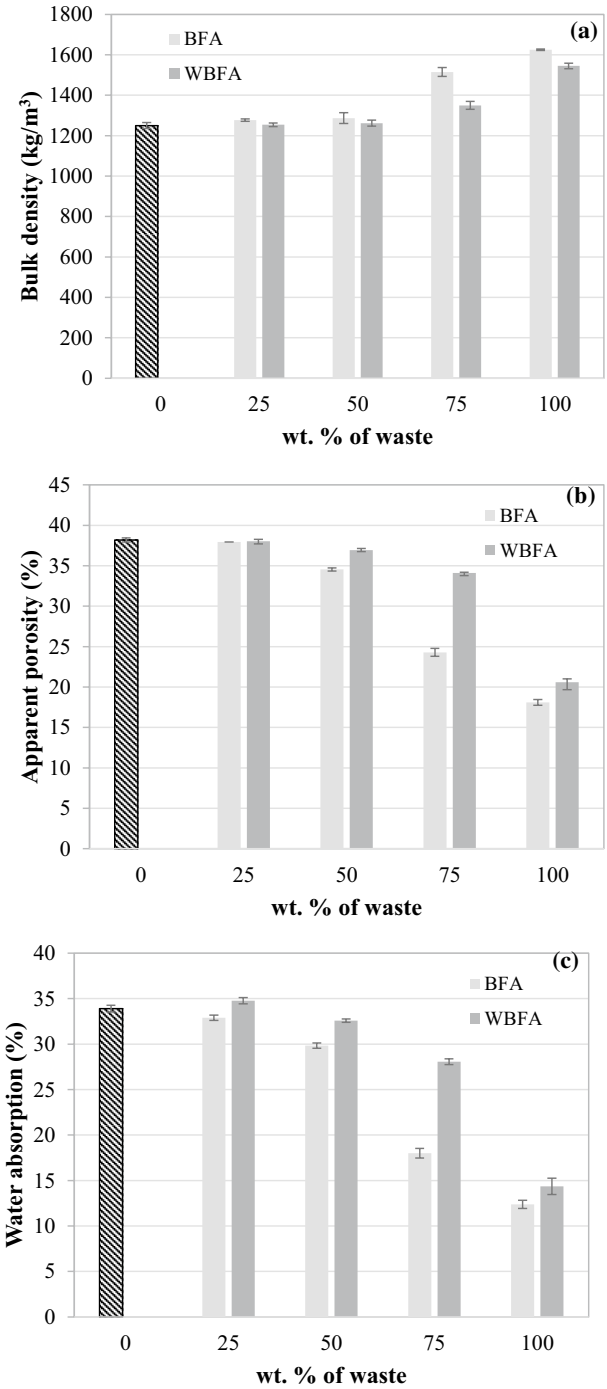

Fig. 7 Bulk density, apparent porosity and water absorption of alkali-activated bricks after 28 days of curing as function of wt% of fly ash (BFA) or washed fly ash (WBFA) incorporated

represents a reduction of 4.8%. Moreover, BFA presents a higher amount of additional alkaline species that could improve the dissolution of the solid precursor resulting in a high polycondensation of Si- and Al-oligomers extending the geopolymer network and improving the densification of the structure. It can justify the decrease of the apparent porosity.

Concerning of the influence of the NaOH concentration of the alkali-activated bricks (Fig. 8) incorporating 50 wt% residue, it can be observed that both bricks samples using BFA and those using WBFA present a lower density as lower NaOH concentrations are used, due to an increase in the *w*/*b* ratio (Table 4). Therefore, the use of a higher amount of water results in higher fluidity and lower paste consolidation, which created pores in the samples that contributed to lower bulk density and higher apparent porosity and water absorption.

3.2 Compressive strength

The mechanical strength in terms of compressive strength of the alkali-activated materials after 28 days of curing is reported in Fig. 9. The 28-days compressive strengths of the specimens are 23.0, 35.9, 44.0, 24.1 and 18.1 MPa for MK,

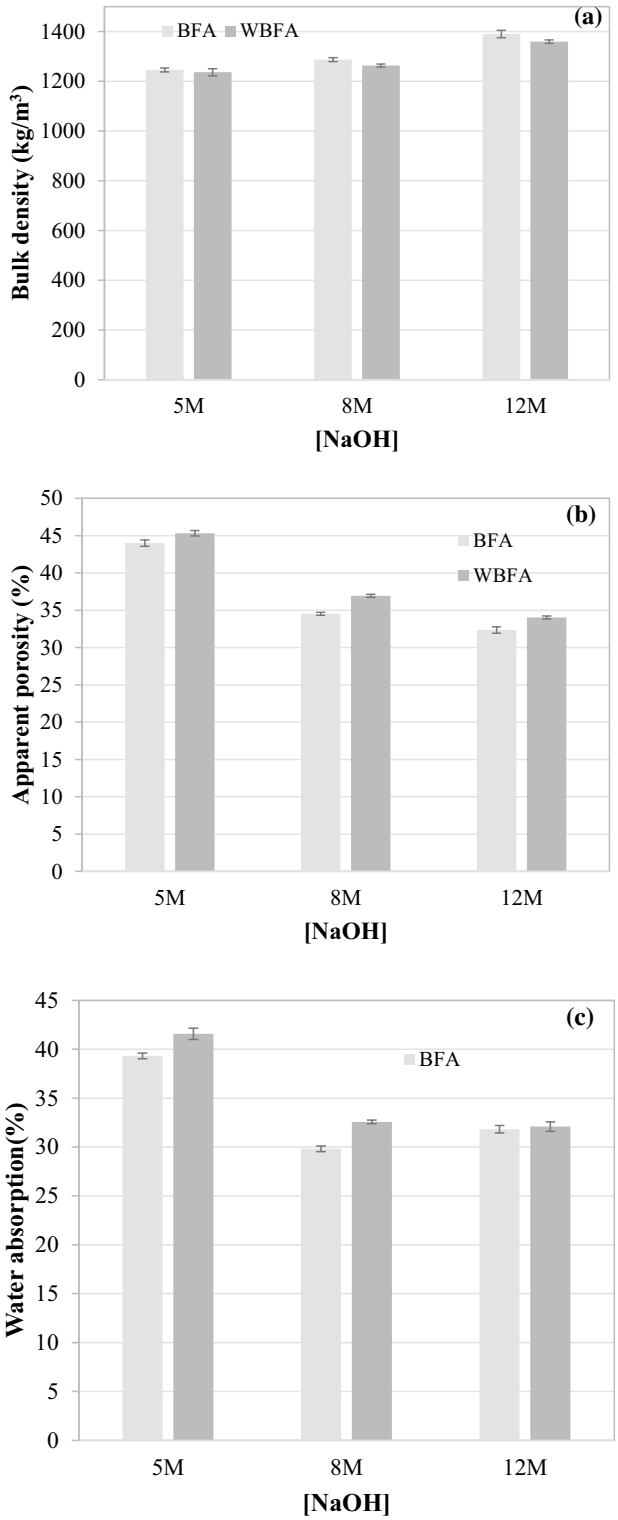

Fig. 8 Bulk density, apparent porosity and water absorption of alkali-activated bricks after 28 days of curing as a function of NaOH concentration with fly ash (50BFA) or washed fly ash (50WBFA) incorporated

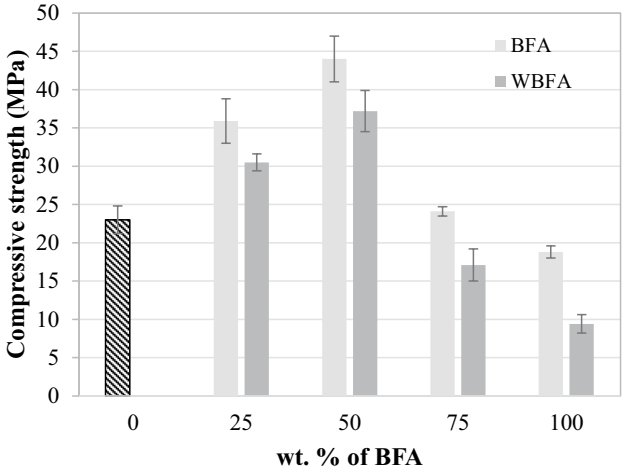

Fig. 9 Compressive strength as function of wt% of fly ash (BFA) or washed fly ash (WBFA) incorporated

25MK-25BFA, 50MK-50BFA, 25MK-75BFA and 100BFA, respectively. The compressive strength increases with the addition of BFA up to 50 wt% and decreases. The increase in compressive strength with the increase of up to 50 wt% of BFA can be explained due to the presence of calcium in the ashes that will react with silicate and aluminate to form various forms of calcium silicate hydrates and calcium aluminum hydrates C–S (A)–H gel. This gel fill the voids and pores of the geopolymeric binder N(K)–Al–Si–H, which increases the density of the paste increasing the compressive strength [44]. Therefore, the addition of ash decreases porosity of the different hydrated phases, which can lead to an increase in the mechanical strength of these specimens. The CaO content of ashes could develop the dissolution of the glassy phase and then facilitates the polymerization reaction. The simultaneous formation of geopolymer and CSH gel help to bridge the gaps between the different hydrated phases and the unreacted particles, resulting in a denser and more homogeneous matrix. The formation of CSH gel within a geopolymeric binder functions as a microaggregate. In this way, the compressive strength of specimens containing up to 50 wt% of BFA increases. However, when ash amounts of 75–100 wt% are added, the excessive calcium content can induce the formation of calcium-based products, leading to a decrease in the strong Si–O–Al bonding in the geopolymer system, resulting in a decrease in compressive strength [45]. It is generally accepted that the presence of excess calcium hydroxide in the resulting structure and the subsequent carbonation process are one of the main causes of concrete deterioration [46]. In addition, ash is rich in organic matter, as indicated by the LOI value (Table 2), so this addition

increases the organic content in the matrix. With the addition of 75 and 100 wt% of the residue the amount of organic matter can be significant and it would limit polycondensation reaction, increasing the setting time with consequent loss of mechanical strength [47].

When using ashes subjected to washing pretreatment, lower compressive strength values obtained, decreasing between 15% and 50% for the 75MK-25WBFA and 100WBFA specimens with respect to the same 75MK-25BFA and 100BFA alkali-activated bricks, respectively. When ashes are rich in alkalis improve the dissolution of the MK precursor and the BFA residue, resulting in a higher extension of the geopolymer network structure leading to higher compressive strength of the specimens employing unwashed ashes.

The influence of NaOH solution concentration on compressive strength is shown in Fig. 10. As can be seen, the compressive strength increases as the NaOH concentration increases. The increase is greater from 5 to 8 M. Increasing the concentration up to 12 M does not produce significant improvements in compressive strength. The geopolymerization reaction is accelerated with a more concentrated alkaline environment. The presence of higher amounts of hydroxyl ions will improve the dissociation of silicate and aluminate and further polymerization. On the other hand, a higher *w*/*b* ratio in the samples was unfavorable for the development of mechanical strength. One of the reasons for the loss of compressive strength is the higher porosity of the samples due to the larger space between the particles and their lower cohesion associated to the low alkalinity of the matrix. Depending on the alkalinity of the system, it is possible that the formation of geopolymer gel and CSH gel compete with each other. Therefore, instead of having one phase acting as a microaggregate to fill the voids and gaps

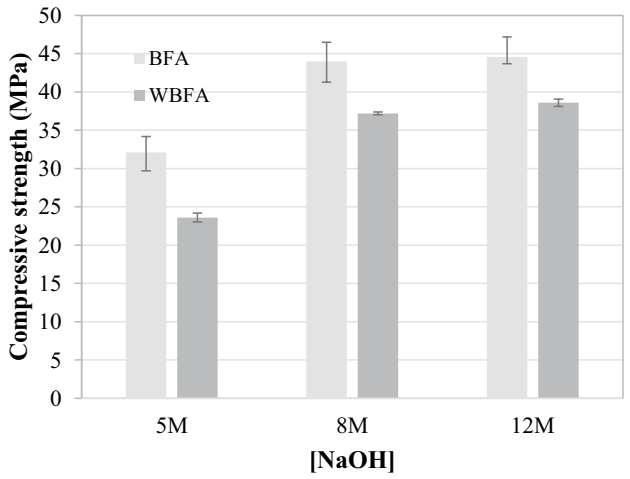

Fig. 10 Compressive strength as function of NaOH concentration with fly ash (50BFA) or washed fly ash (50WBFA) incorporated

in the binder, two reactions compete for soluble silicates and space available for growth. Consequently, resulting binder will be disordered with two phases of similar size, resulting in increased porosity, leading to a reduction in compressive strength in the specimens using a 5 M NaOH concentration. When 8 and 12 M dilution is employed, the formation of CSH gel and geopolymer gel can take place simultaneously. The amount and nature of the final products will depend mainly on the ratio between aluminosilicate and calcium sources, as well as the alkalinity of the alkaline activators [44]. The low increase observed when increasing the concentration from 8 to 12 M may be due to the fact that the higher OH^- concentration may lead to $Ca(OH)_2$ precipitation and inhibition of C–(A)–S–H gel formation. In general, the use of high-molarity NaOH has economic, environmental and safety limitations in the application of building materials. Therefore, it can be deduced that the optimum molarity of NaOH for the activation of 50MK-50BFA precursors is 8 M.

3.3 X-ray diffraction (XRD)

The XRD pattern of the control 100MK and alkali-activated bricks containing different amounts (25–100 wt%) of the BFA residue are presented in Fig. 11. In the X-ray patterns, the X-ray hump is observed between 20–40° (2θ). This hump appears in the metakaolin precursor from 15–35 (2θ), while in the BFA residue from 20–35° (2θ). The shift of this hump towards higher 2θ indicates the formation of the amorphous N–A–S–H geopolymeric gel [48–51]. A significant decrease of this amorphous halo can be observed for the 25MK-75BFA and 100BFA alkali-activated bricks, confirming the higher degree of polycondensation of these specimens. In addition to the formation of amorphous binder, the diffraction pattern of the 100MK at 28 days of curing indicates the diffraction peaks of quartz present in the precursor, as well as the presence of traces of calcite due to its carbonation. In alkali-activated bricks incorporating different amounts of the BFA residue (25–100 wt%), diffraction peaks corresponding to quartz, present in both precursors, and calcite, present in the BFA residue, are observed. This suggests that most of these crystalline phases do not react or partially react during the geopolymerization process due to the decrease in intensity. The diffraction peaks corresponding to sylvite and aluminosilicates are not observed implying that these minerals dissolve in the alkaline medium during the geopolymerization process and form new phases. The amorphous C–S–H and C–A–S–H cementitious products are difficult to observe, due to the interference between peaks of the different phases, since these phases appear as diffuse diffraction peaks at angles approximately 28–30, 34 and 35° (2θ) [52].

Regarding the influence of the washing pretreatment, the XRD pattern of the alkali-activated bricks 50MK-50BFA and 50MK-50WBFA is shown as an example (Fig. 12). It

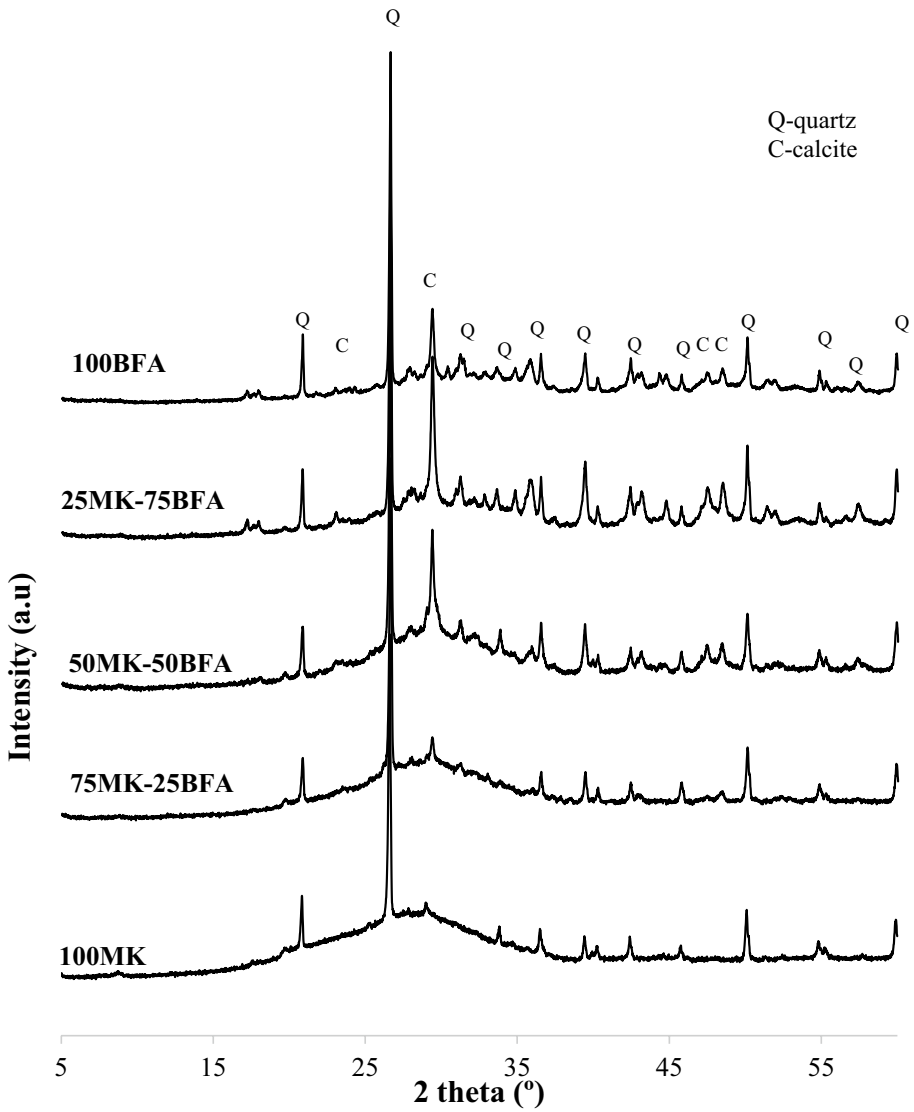

Fig. 11 XRD patterns of alkali-activated bricks as a function of wt% of fly ash and control bricks (100MK)

shows that there are no differences in both diffraction patterns, with the diffraction peak of quartz being slightly more intense in 50MK-50WBFA bricks, indicating a lower reaction. As for the influence of NaOH concentration (Fig. 13) no differences are observed in the diffraction patterns of the 5 and 8 M bricks. Increasing the concentration up to 12 M causes the excess sodium ions in the medium to react with calcium carbonate forming calcium sodium carbonate.

3.4 Fourier transform infrared spectroscopy (FTIR)

Figure 14 shows the FTIR spectra of alkali-activated bricks incorporating different amounts of BFA residue (25–100 wt%) after 28 days of curing. The absorption bands centered between 3211 and 3366 cm^{-1} and at 1645 cm^{-1} are assigned as indicated in the WBFA precursor to the –OH bond stretching vibrations and the H–O–H bending vibrations of the bound water molecules, respectively. These bands proceed from water molecules adsorbed on the surface or trapped in cavities of the geopolymer structures [53]. The intensity of these bands decreases with the addition of higher amounts of BFA (75–100 wt%). This indicates a lower degree of adsorption of water molecules from these alkali-activated bricks or less gel formation. The bands centered at approximately 1450 and 870 cm^{-1} in all alkali-activated bricks are attributed to vibrations of the O–C–O bonds in the carbonate molecules, asymmetric stretching and bending, respectively [54, 55]. These bands are related to the carbonation reaction of the samples during synthesis and curing. They are more intense in alkali-activated bricks with higher BFA content (75 and 100 wt%), so it could also be assigned to the carbonate content present in the residue [56, 57]. A shift of the main band from 1058 cm^{-1} for the MK precursor to 973 cm^{-1} for the 100MK bricks is observed after 28 days

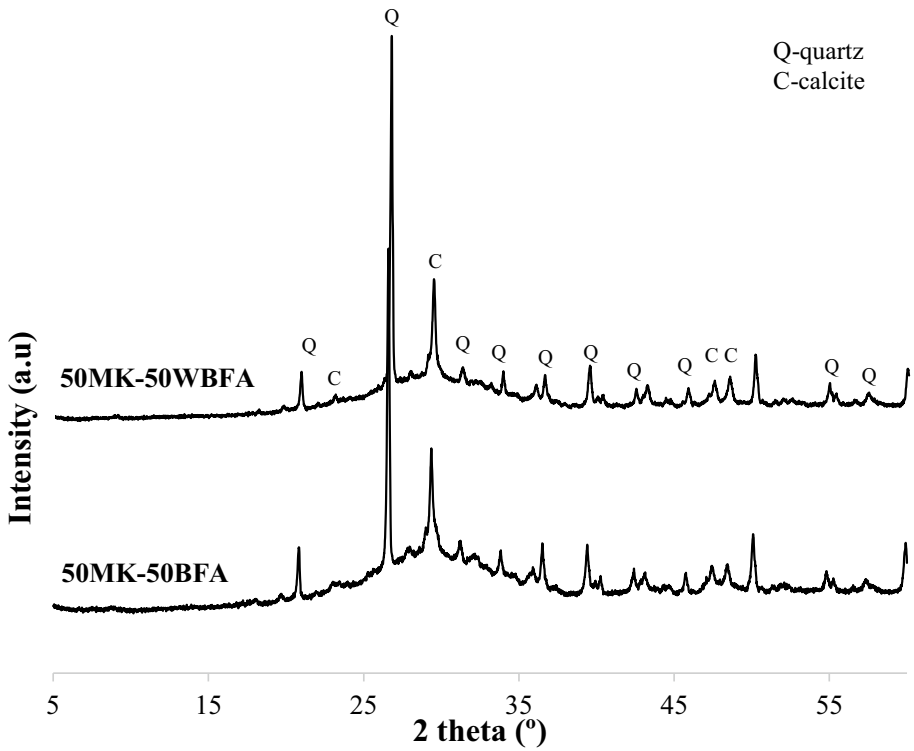

Fig. 12 XRD patterns of 50WBFA and 50BFA alkali-activated bricks

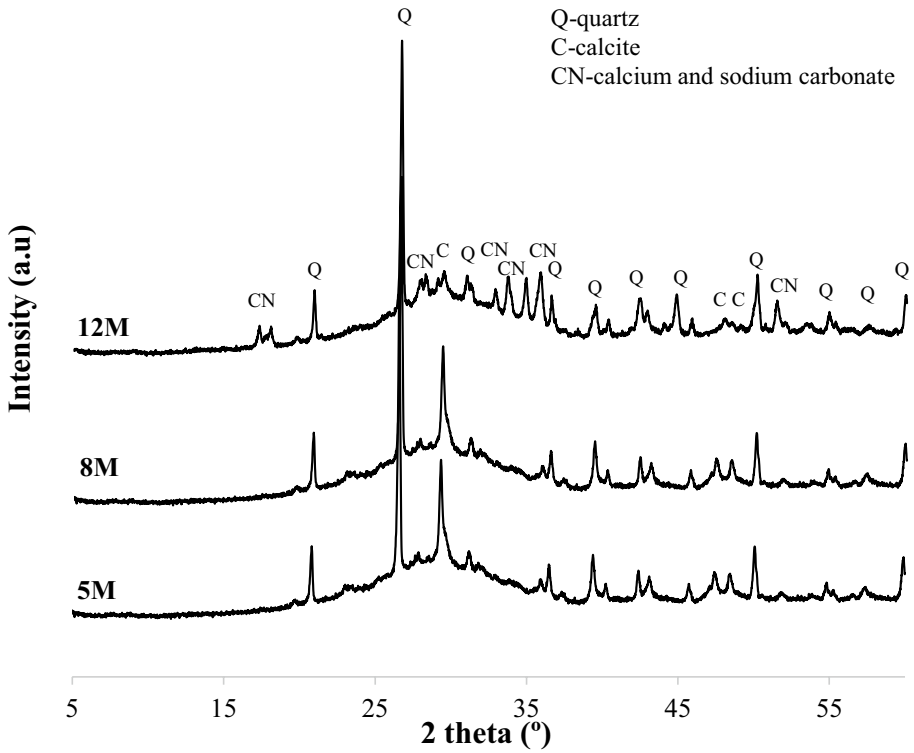

Fig. 13 XRD patterns of 50BFA as function of NaOH concentration

of curing. The addition of 25–50 wt% BFA produced a shift to lower wavenumbers 969–968 cm^{-1}, increasing to 976 and 977 cm^{-1} with the addition of 75–100 wt% BFA, respectively. This band can be attributed to the vibration of the silicate species bound to the alkaline activator [58–60]. Therefore, the shift of this band indicates the successful

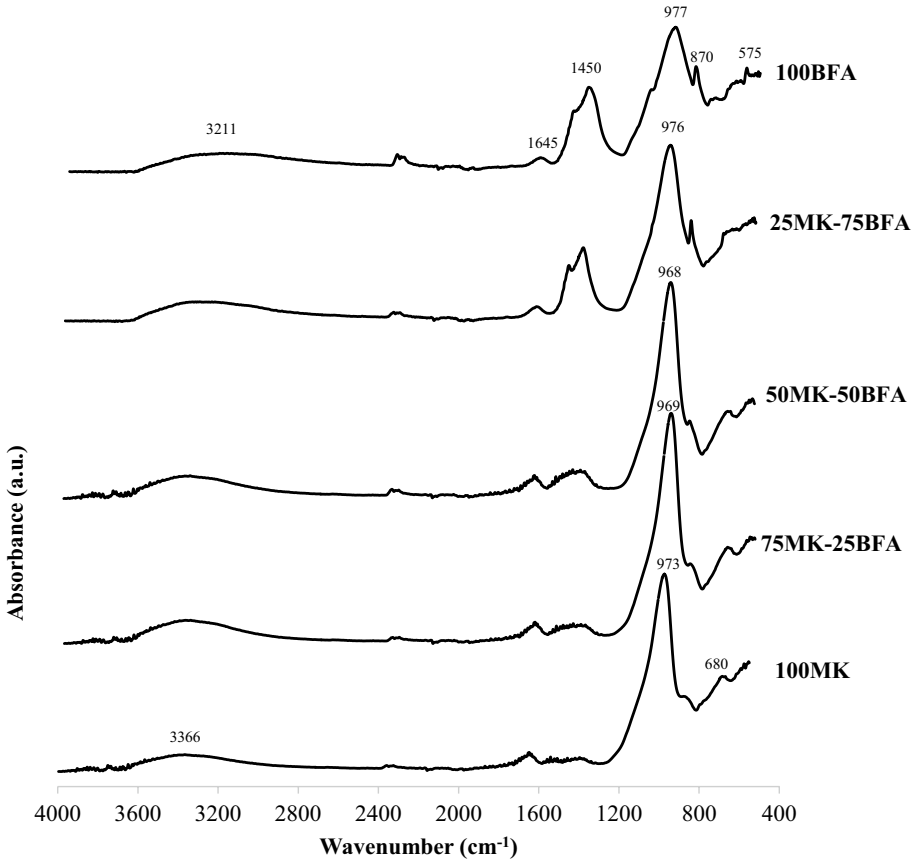

Fig. 14 FTIR spectra as function of wt% of BFA and 100MK control alkali-activated bricks

geopolymerization of the precursors with the addition of activating solution, forming new amorphous products constituting the geopolymer matrix [61]. It is important to note that the intensity of this band is reduced when high amounts of BFA (75–100 wt%) are used, which could indicate the lower formation of geopolymer gel, due to the lower amount of Si–O–T groups (Si, Al) when high amounts of residue are added [53, 62]. The absorption bands observed at 680 cm^{-1} are attributed to the bending vibration of the Si–OSi–O–Si bonds of quartz, indicating weak dissolution of the quartz phases in alkaline medium. The band centered at 575 cm^{-1} is assigned to the vibration of Al–O bonds [63].

As for the influence of the washing pretreatment only a slight shift of the bands centered at 968 and 977 cm^{-1} is observed for the geopolymeric bricks 50MK-50BFA and 100BFA, respectively up to 971 and 985 cm^{-1} for the alkali-activated bricks 50MK-50WBFA and 100WBFA respectively (Fig. 15). This shift to higher wavenumbers could be due to lower amount of alkali ions provided by pretreated samples. Therefore, the negative charges of the Al species inserted in the tetrahedral Si site of the geopolymer network could be compensated by the positive alkali ions, K^+, Ca^{2+}, present in the BFA, modifying the intramolecular distances in accordance with Deutou Nemaleu et al. [47].

Concerning the FTIR spectra of the 50MK-50BFA alkali-activated bricks in which different concentrations of NaOH are used as activating solution (Fig. 16), a shift of the band assigned to the asymmetric stretching vibration of the Si–O–T group can be observed, centered at 980 cm^{-1} for the specimens using 5 M solution up to 968 cm^{-1} for the samples using 8 and 12 M solution. The larger shift of the main band towards lower wavenumbers when higher NaOH concentrations are used could be related to the increase of the amorphous phase in the alkali-activated cement structure. It implies an increase in the degree of geopolymerization, due to a higher dissolution of MK and BFA precursors and a higher substitution of Si–OSi–O–Si by Si–O–Al at the tetrahedral sites with the provision of more nucleation sites in the three-dimensional geopolymer structure leading to a local change of the Si–O bond environment [64, 65].

3.5 Scanning electron microscope coupled by energy-dispersive X-ray spectroscopy (SEM–EDS)

The SEM images and EDS analysis of the selected alkali-activated bricks are shown in Fig. 17. The control specimens 100MK presents a large number of pores and the presence of

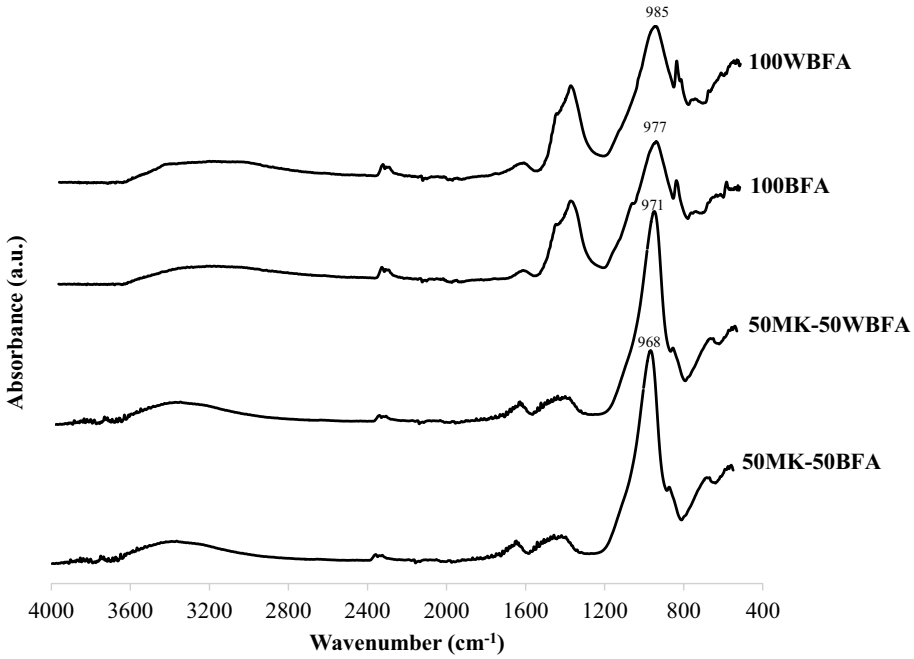

Fig. 15 FTIR spectra of 50MK-50BFA, 50MK-50WBFA, 100BFA and 100 WBFA alkali-activated bricks

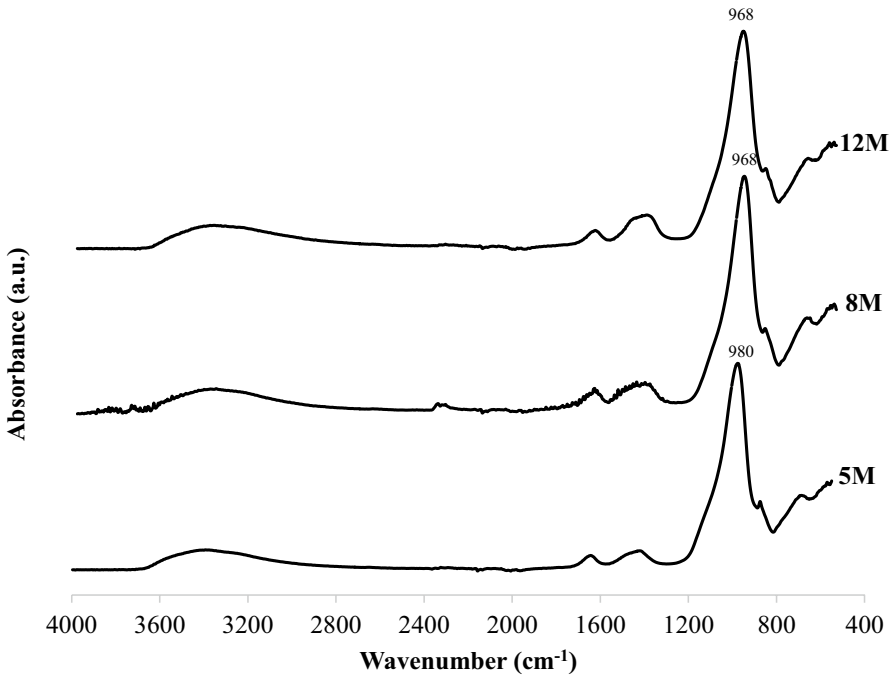

Fig. 16 FTIR spectra of 50MK-50BFA alkali-activated bricks as function of NaOH concentration

Si, Al and Na, which is ascribed to the poly-(sialate-siloxo) networks called N–A–S–H geopolymeric gel [66, 67] as indicated by the EDS (Spectrum 1). The substitution of MK precursor by BFA residue results in a denser structure with lower porosity, with unreacted ash particles (Spectrum 2) observed in higher proportion in the 100BFA specimens embedded in voids or connected with the main amorphous gel matrix. The shrinkage between unreacted particles results in formation of microcracks, which are responsible for microstructural defects and loss of compressive strength. The addition of BFA indicates the participation of Ca^{2+} ions contained in the precursor in the geopolymerization reactions giving rise to a mixed amorphous (N, C)–A–S–H gel due to the combination of C–A–S–H and N–A–S–H gel [62]. The existence of (N, C)–A–S–H gel exhibits a soft and dense matrix, giving the sample 50MK-50BFA with a stronger structure. BFA activation results in a (C, N)–A–S–H gel richer in calcium than in sodium (Spectrum 4) and with a

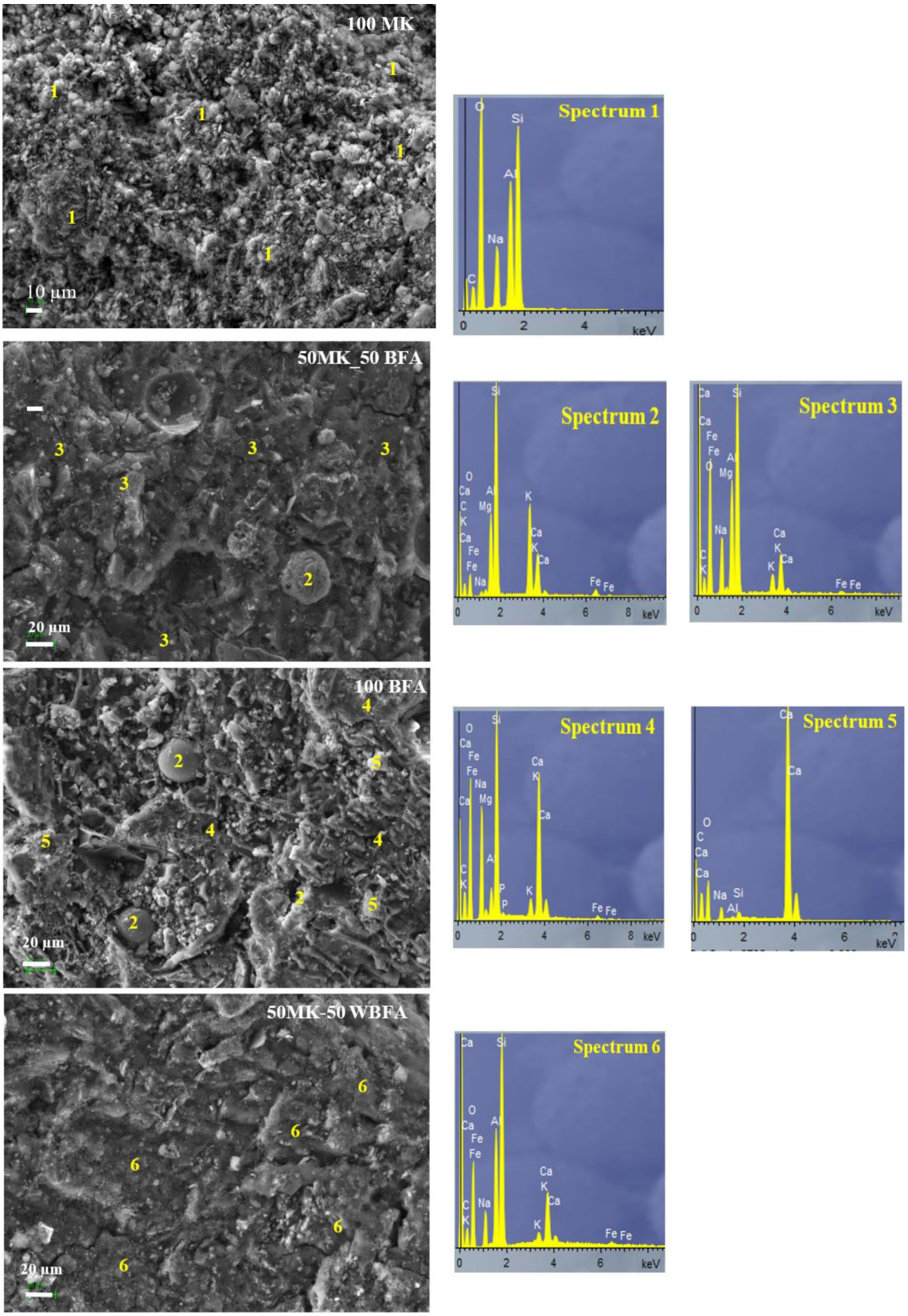

Fig. 17 SEM–EDS results of selected alkali-activated bricks: 100 MK; 50MK-50BFA; 100BFA; 50-50WBFA; 50MK-50BFA-5M and 50MK-50BFA-12M at 1000× magnification

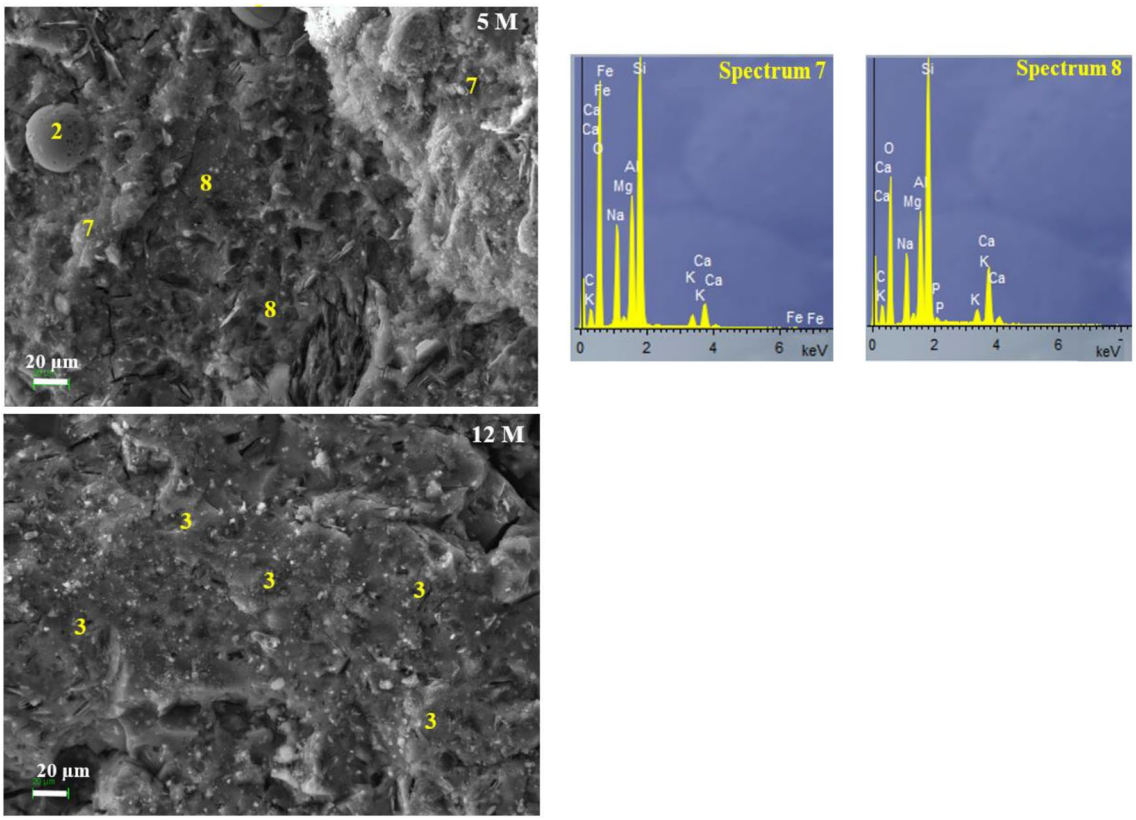

Fig. 17 (continued)

relative lower amount of aluminum. In addition, unreacted calcium-rich particles are observed (Spectrum 5), although a large proportion of the calcium components contained in BFA precursor participate in formation of gel structure. The amount of unreacted particles is higher in the 100BFA alkali-activated bricks, resulting in lower amount of geopolymeric gel which justifies the loss of compressive strength with additions above 50 wt% residue.

In the SEM micrographs of the alkali-activated bricks 50MK-50WBFA using ashes subjected with a washing pretreatment as precursor, no major differences are observed with respect to the bricks 50MK-50BFA. The formation of the mixed gel (N, C)–A–S–H (Spectrum 6) can be observed presenting a greater amount of pores and shrinkage microcracks, indicating a worse progress of the geopolymerization reaction.

Regarding the influence of NaOH concentration, it can be observed that when the NaOH concentration is low, 5 M, the coexistence of two separate phases takes place. One zone rich in silica, aluminum and sodium, with a very small amount of calcium (Spectrum 7) and structure similar to that obtained by alkaline activation of metakaolin, N–A–S–H geopolymer gel, and another zone with dominance of silica, aluminum, calcium and sodium, indicating (C,N)–A–S–H formation (Spectrum 8). The coexistence of both N–A–S–H and C–A–S–H gels results in a weaker structure, due to competition in formation, resulting in less dense and less homogeneous structure due to the separation of both phases and unreacted particles, as indicated by the compressive strength data, neither phase acting as a microaggregate to fill holes and voids of the binder [68, 69]. However, the coexistence of both gels disappears when a higher alkalinity or higher concentration of NaOH, 8 M and 12 M, is used, being the major product formed the mixed (C, N)–A–S–H gel (Spectrum), giving rise to denser and more homogeneous structures with higher compressive strength values.

4 Conclusions

The performance of metakaolin-based alkali-activated bricks, which different amounts of BFA (25–100 wt%) added in alkaline medium has been investigated. In addition, the effect of the alkali content in the ash precursor, by subjecting to a washing pretreatment (WBFA) and of the NaOH concentration on the physical, mechanical and microstructural properties on bricks has been studied. From the results, the following main conclusions are drawn:

- Bulk density increases, water absorption and apparent porosity decrease with the addition of higher amounts of the BFA residue. The washing pretreatment, as well as the use of low NaOH concentrations, results in alkali-activated bricks with lower density and with higher bulk porosity and water absorption.
- The substitution of metakaolin by 50 wt% BFA resulted in an increase in compressive strength, due to the formation of a homogeneous mixed gel (N, C)–A–S–H that contributes to the increase in compressive mechanical strength. The content of soluble salts in the ashes has positive effect on the mechanical properties, resulting in higher extension of the geopolymer network structure. The NaOH concentration has a marked effect on the mechanical properties. Low NaOH concentrations result in the formation of a disordered heterogeneous matrix with two N–A–S–H and C–S–H gels of higher porosity, leading to reduction in compressive strength.
- XRD patterns and the observed shift in FTIR spectra confirm a higher formation of amorphous gel network structure for samples incorporating up to 50 wt% BFA. Higher BFA incorporations (75–100 wt%), washing pretreatment and low NaOH concentrations result in a decrease of the geopolymerization reaction. In consequence, a decrease in mechanical properties is produced.

Therefore, this research demonstrates that the substitution of 50 wt% MK for 50 wt% BFA results in alkali-activated bricks with improved mechanical properties. The alkali content of the ashes contributes to an increase in compressive strength, and an 8 M or higher NaOH concentration is required to obtain optimum mechanical properties. Future durability studies in different environments, economic and environmental performance will be carried out to determine its viability as structural materials in civil engineering with economic and environmental benefits over other conventional building materials.

Acknowledgements This work has been funded by the project «Development and characterization of new geopolymerical composites based on waste from the olive industry. Towards a sustainable construction (MAT2017-88097-R)», FEDER/Ministry of Science, Innovation and Universities, State Research Agency and the project «PID2020-115161RB-I00: Applying the circular economy in the development of new low carbon footprint alkaline activated hydraulic binders for construction solutions (CongActiva)» funded by MCIN/AEI/10.13039/501100011033FEDER "A way of making Europe". The authors thank to the companies "Caobar S.A." and "Aldebarán Energía del Guadalquivir S.A." for supplying the kaolin and biomass fly ash, respectively. Technical and human support provided by CICT of Universidad de Jaén (UJA, MINECO, Junta de Andalucía, FEDER) are gratefully acknowledged.

Author contributions SJ-C: investigation, data curation, methodology, preparation and treatment of figures, and analysis of data. Writing—review and editing. EB-M: investigation, data curation, performed some determinations and test. PJS-S: conceptualization, methodology, data curation, validation, formal analysis, writing—review and editing. OG: data curation, validation, formal analysis, writing—review and editing. DE-Q: conceptualization, formal analysis, investigation, data curation, resources, supervision, project administration, funding acquisition, visualization, writing–original draft, writing—review and editing.

Funding Open Access funding provided thanks to the CRUE-CSIC (Universidad de Jaén/CBVA) agreement with Springer Nature. This work has been funded by the project "Development and characterization of new geopolymerical composites based on waste from the olive industry. Towards a sustainable construction (MAT2017-88097-R)", FEDER/Ministry of Science, Innovation and Universities, State Research Agency and the project "PID2020-115161RB-I00: Applying the circular economy in the development of new low carbon footprint alkaline activated hydraulic binders for construction solutions (CongActiva)" funded by MCIN/AEI/10.13039/501100011033FEDER "A way of making Europe".

Declarations

Conflict of interest The authors declare that they have no known competing financial interests or personal relationships that could have appeared to influence the work reported in this paper.

Ethics approval Not applicable.

Consent, data, materials and/or code availability The data will be provided upon reasonable request to the authors.

References

1. Hashmi AF, Shariq M, Baqi A. Flexural performance of high volume fly ash reinforced concrete beams and slabs. Structures. 2020;25:868–80. https://doi.org/10.1016/j.istruc.2020.03.071.
2. Hashmi AF, Shariq M, Baqi A. An investigation into age-dependent strength, elastic modulus and deflection of low calcium fly ash concrete for sustainable construction. Constr Build Mater. 2021;283: 122772. https://doi.org/10.1016/j.conbuildmat.2021.122772.
3. Rashad AM. Alkali-activated metakaolin: a short guide for civil engineer–an overview. Constr Build Mater. 2013;41:751–65. https://doi.org/10.1016/j.conbuildmat.2012.12.030.
4. Sarker PK, Kelly S, Yao Z. Effect of fire exposure on cracking, spalling and residual strength of fly ash geopolymer concrete. Mater Des. 2014;3:584–92. https://doi.org/10.1016/j.matdes.2014.06.059.

5. Hassan A, Arif M, Shariq M. Use of geopolymer concrete for a cleaner and sustainable environment—a review of mechanical properties and microstructure. J Clean Prod. 2019;223:704–28. https://doi.org/10.1016/j.jclepro.2019.03.051.
6. Zhang Z, Wang H, Zhu Y, Reid A, Provis JL, Bullen F. Using fly ash to partially substitute metakaolin in geopolymer synthesis. Appl Clay Sci. 2014;88–89:194–201. https://doi.org/10.1016/j.clay.2013.12.025.
7. Villaquirán-Caicedo MA, Mejía de Gutiérrez R, Sulekar S, Davis C, Nino JC. Thermal properties of novel binary geopolymers based on metakaolin and alternative silica sources. Appl Clay Sci. 2015;118:276–82. https://doi.org/10.1016/j.clay.2015.10.005.
8. Guo X, Xiong G. Resistance of fiber-reinforced fly ash-steel slag based geopolymer mortar to sulfate attack and drying-wetting cycles. Constr Build Mater. 2021;269:121326. https://doi.org/10.1016/j.conbuildmat.2020.121326.
9. Apithanyasai S, Supakata N, Papong S. The potential of industrial waste: using foundry sand with fly ash and electric arc furnace slag for geopolymer brick production. Heliyon. 2020;6: e03697. https://doi.org/10.1016/j.heliyon.2020.e03697.
10. Atabey I, Karahan O, Bilim C, Atiş CD. The influence of activator type and quantity on the transport properties of class F fly ash geopolymer. Constr Build Mater. 2020;264: 120268. https://doi.org/10.1016/j.conbuildmat.2020.120268.
11. Freire AL, Moura-Nickel CD, Scaratti G, De Rossi A, Araújo MH, De Noni JA, Rodrigues AE, Rodríguez-Castellón E, Moreira R. Geopolymers produced with fly ash and rice husk ash applied to CO_2 capture. J Clean Prod. 2020;273: 122917. https://doi.org/10.1016/j.jclepro.2020.122917.
12. La bioenergía en Andalucía. In: Agencia Andaluza de la Energía. Consejería de Hacienda, Industria y Energía. 2020. https://www.agenciaandaluzadelaenergia.es/sites/default/files/Documentos/3_2_0068_20_LA_BIOENERGIA_EN_ANDALUCIA.PDF. Accessed 3 Jan 2020
13. Nogales R, Delgado G, Quirantes M, Romero M, Romero E, Molina-Alcaide E. Characterization of olive waste ashes as fertilizers. In: Insam H, Knapp BA, editors. Recycling of biomass ashes. Heidelberg: Springer; 2011. p. 57–68.
14. Cuenca J, Rodríguez J, Martín-Morales M, Sánchez-Roldán Z, Zamorano M. Effects of olive residue biomass fly ash as filler in self-compacting concrete. Constr Build Mater. 2013;40:702–9. https://doi.org/10.1016/j.conbuildmat.2012.09.101.
15. Cruz-Yusta M, Mármol I, Morales J, Sánchez L. Use of olive biomass fly ash in the preparation of environmentally friendly mortars. Environ Sci Technol. 2011;45:6991–6.
16. Fernández-Pereira C, de la Casa JA, Gómez-Barea A, Arroyo F, Leiva C, Luna Y. Application of biomass gasification fly ash for brick manufacturing. Fuel. 2011;90:220–32. https://doi.org/10.1016/j.fuel.2010.07.057.
17. Eliche-Quesada D, Felipe-Sesé MA, Moreno-Molina AJ, Franco F, Infantes-Molina A. Investigation of using bottom or fly pine-olive pruning ash to produce environmental friendly ceramic materials. Appl Clay Sci. 2017;135:333–46. https://doi.org/10.1016/j.clay.2016.10.015.
18. Hinojosa MJR, Galvín AP, Agrela F, Perianes M, Barbudo A. Potential use of biomass bottom ash as alternative construction material: conflictive chemical parameters according to technical regulations. Fuel. 2014;128:248–59. https://doi.org/10.1016/j.fuel.2014.03.017.
19 Munawar MA, Khoja AH, Naqvi SR, Mehran MT, Hassan M, Liaquat DUF. Challenges and opportunities in biomass ash management and its utilization in novel application. Renew Sustain Energy Rev. 2021;150:111451. https://doi.org/10.1016/j.rser.2021.111451.
20 Knapp BA, Insam H. Recycling of biomass ashes: current technologies and future research needs. In: Insam H, Knapp B, editors. Recycling of biomass ashes. Heidelberg: Springer, Berlin; 2011.
21. Laxman Yadav A, Sairam V, Srinivasan K, Muruganandam L. Synthesis and characterization of geopolymer from metakaolin and sugarcane bagasse ash. Constr Build Mater. 2020;258: 119231. https://doi.org/10.1016/j.conbuildmat.2020.119231.
22. Nana A, Epey N, Kaze C, Deutou JG, Djobo JN, Sylvain T, Alomayri TS, Ngounéa J, Kamseub E, Leonellif C. Mechanical strength and microstructure of metakaolin/volcanic ash-based geopolymer composites reinforced with reactive silica from rice husk ash (RHA). Materialia. 2021;16: 101083. https://doi.org/10.1016/j.mtla.2021.101083.
23. De Rossi A, Simão L, Ribeiro MJ, Hotza D, Moreira RFPM. Study of cure conditions effect on the properties of wood biomass fly ash geopolymers. J Mater Res Technol. 2020;9(4):7518–28. https://doi.org/10.1016/j.jmrt.2020.05.047.
24. Perná I, Šupová M, Hanzlíček T, Špaldoňová A. The synthesis and characterization of geopolymers based on metakaolin and high LOI straw ash. Constr Build Mater. 2019;228: 116765. https://doi.org/10.1016/j.conbuildmat.2019.116765.
25. Yurt Ü, Bekar F. Comparative study of hazelnut-shell biomass ash and metakaolin to improve the performance of alkali-activated concrete: a sustainable greener alternative. Constr Build Mater. 2022;320: 126230. https://doi.org/10.1016/j.conbuildmat.2021.126230.
26. Rajamma R, Labrincha JA, Ferreira VM. Alkali activation of biomass fly ash–metakaolin blends. Fuel. 2012;98:265–71. https://doi.org/10.1016/j.fuel.2012.04.006.
27. De Aza AH, Turrillas X, Rodríguez MA, Durana T, Peña P. Time-resolved powder neutron diffraction study of the phase transformation sequence of kaolinite to mullite. J Eur Ceram Soc. 2014;34:1409–21. https://doi.org/10.1016/j.jeurceramsoc.2013.10.034.
28 Fernández-Jiménez A, Monzo M, Vicent M, Barba A, Palomo A. Alkaline activation of metakaolin–fly ash mixtures: obtain of zeoceramics and zeocements. Micropor Mesopor Mater. 2008;108:41–9. https://doi.org/10.1016/j.micromeso.2007.03.024.
29. Granizon N, Palomo A, Fernandez-Jiménez A. Effect of temperature and alkaline concentration on metakaolin leaching kinetics. Ceram Int. 2014;40:8975–85. https://doi.org/10.1016/j.ceramint.2014.02.071.
30. Kouamo HT, Mbey JA, Elimbi A, Diffo BB, Njopwouo D. Synthesis of volcanic ash-based geopolymer mortars by fusion method: effects of adding metakaolin to fused volcanic ash. Ceram Int. 2013;39:1613–21. https://doi.org/10.1016/j.ceramint.2012.08.003.
31. Van Jaarsveld JGS, Van Deventer JSJ, Lukey GC. The characterisation of source materials in fly ash-based geopolymers. Mater Lett. 2003;57(7):1272–80. https://doi.org/10.1016/S0167-577X(02)00971-0.
32. Vassilev SV, Baxter D, Andersen LK, Vassileva CG. An overview of the chemical composition of biomass. Fuel. 2019;89:913–33. https://doi.org/10.1016/j.fuel.2009.10.022.
33. Singhal A, Gangwar BP, Gayathry JM. CTAB modified large surface area nanoporous geopolymer with high adsorption capacity for copper ion removal. Appl Clay Sci. 2017;150:106–14. https://doi.org/10.1016/j.clay.2017.09.013.
34. Tchakouté HK, Melele SJK, Djamen AT, Kaze CR, Kamseu E, Nanseu CNP, Leonelli C, Ruscher CH. Microstructural and mechanical properties of poly(sialatesiloxo) networks obtained using metakaolins from kaolin and halloysite as aluminosilicate sources: a comparative study. Appl Clay Sci. 2020;186:105448–59. https://doi.org/10.1016/j.clay.2020.105448.
35 Ramachandran VS, Paroli RM, Beaudoin J, Delgado AH. Handbook of thermal analysis of construction materials. Thermochim

Acta. 2003;406:209. https://doi.org/10.1016/S0040-6031(03)00230-2.
36. Rozek P, Krol M, Mozgawa W. Spectroscopic studies of fly ash-based geopolymers. Spectrochim Acta A Mol Biomol Spectrosc. 2018;198:283–9. https://doi.org/10.1016/j.saa.2018.03.034.
37. Ozer I, Soyer-Uzun S. Relations between the structural characteristics and compressive strength in metakaolin based geopolymers with different molar Si/Al ratios. Ceram Int. 2015;41:10192–8. https://doi.org/10.1016/j.ceramint.2015.04.125.
38. Kouamo HT, Elimbi A, Mbey JA, Ngally-Sabouang CJ, Njopwouo D. The effect of adding alumina-oxide to metakaolin and volcanic ash on geopolymer products: a comparative study. Constr Build Mater. 2012;35:960–9. https://doi.org/10.1016/j.conbuildmat.2012.04.023.
39. UNE-EN ISO 17294-1:2007 (2007) Water quality—application of inductively coupled plasma mass spectrometry (ICP-MS)—part 1: general guidelines (ISO 17294-1:2004)
40. UNE-EN ISO 17294-2:2017 (2017) Water quality—application of inductively coupled plasma mass spectrometry (ICP-MS)—part 2: determination of selected elements including uranium isotopes (ISO 17294-2:2016)
41. UNE-EN 1015-10:2000/A1:2007 (2007) Methods of test for mortar for masonry—part 10: determination of dry bulk density of hardened mortar
42. ASTM C642-13 (2016) Standard test method for density, absorption, and voids in hardened concrete. ASTM International
43. UNE-EN 772-1:2011 (2011) Methods of test for masonry units—part 1: determination of compressive strength
44. Yip CK, Lukey GC, van Deventer JSJ. The coexistence of geopolymeric gel and calcium silicate hydrate at the early stage of alkaline activation. Cem Concr Res. 2005;35(9):1688–97. https://doi.org/10.1016/j.cemconres.2004.10.042.
45. Zhao X, Liu C, Zuo L, Wang L, Zhu Q, Wang M. Investigation into the effect of calcium on the existence form of geopolymerized gel product of fly ash based geopolymers. Cem Concr Compos. 2019;103:279–92. https://doi.org/10.1016/j.cemconcomp.2018.11.019.
46. Yang M, Paudel SR, Asa E. Comparison of pore structure in alkali-activated fly ash geopolymer and ordinary concrete due to alkali-silica reaction using microcomputed tomography. Constr Build Mater. 2020;236: 117524. https://doi.org/10.1016/j.conbuildmat.2019.117524.
47. DeutouNemaleu JG, Kaze RC, Tome S, Alomayri T, Assaedi H, Kamseu E, Melo UC, Sglavo VM. Powdered banana peel in calcined halloysite replacement on the setting times and engineering properties on the geopolymer binders. Constr Build Mater. 2021;279: 122480. https://doi.org/10.1016/j.conbuildmat.2021.122480.
48. Xie N, Bell JL, Kriven WM. Fabrication of structural leucite glass-ceramics from potassium-based geopolymer precursors. J Am Ceram Soc. 2010;93(9):2644–9. https://doi.org/10.1111/j.1551-2916.2010.03794.x.
49. Fernández-Jiménez A, Cristelo N, Miranda T, Palomo Á. Sustainable alkali-activated materials: precursor and activator derived from industrial wastes. J Clean Prod. 2017;162:1200–9. https://doi.org/10.1016/j.jclepro.2017.06.151.
50. Timakul P, Rattanaprasit W, Aungkavattana P. Improving compressive strength of fly ash-based geopolymer composites by basalt fibers addition. Ceram Int. 2016;42(5):6288–95. https://doi.org/10.1016/j.ceramint.2016.01.014.
51. Ozer I, Soyer-Uzun S. Relations between the structural characteristics and compressive strength in metakaolin based geopolymers with different molar Si/Al ratios. Ceram Int. 2015;41(8):10192–8. https://doi.org/10.1016/j.ceramint.2015.04.125.
52. Zhang M, Guo H, El-Korchi T, Zhang G, Tao M. Experimental feasibility study of geopolymer as the next-generation soil stabilizer. Constr Build Mater. 2013;47:1468–78. https://doi.org/10.1016/j.conbuildmat.2013.06.017.
53. Tchakoute HK, Elimbi A, Yanne E, Djangang CN. Utilization of volcanic ashes for the production of geopolymers cured at ambient temperature. Cem Concr Compos. 2013;38:75–81. https://doi.org/10.1016/j.cemconcomp.2013.03.010.
54 Robayo-Salazar RA, Mejía de Gutiérrez R. Natural volcanic pozzolans as an available raw material for alkali-activated materials in the foreseeable future: a review. Constr Build Mater. 2018;189:109–18. https://doi.org/10.1016/j.conbuildmat.2018.08.174.
55. Robayo-Salazar RA, Aguirre-Guerrero AM, MejíadeGutiérrez R. Carbonation-induced corrosion of alkali-activated binary concrete based on natural volcanic pozzolan. Constr Build Mater. 2020;232:117189–11799. https://doi.org/10.1016/j.conbuildmat.2019.117189.
56. Nana A, Alomayri TS, Venyite P, Kaze RC, Assaedi HS, Nobouassia CB, Sontia JVM, Ngouné J, Kamseu E, Leonelli C. Mechanical properties and microstructure of a metakaolin-based inorganic polymer mortar reinforced with quartz sand. Silicon. 2020;14(1):263–74. https://doi.org/10.1007/s12633-020-00816-4.
57. Bayiha BN, Billong N, Yamb E, Kaze RC, Nzengwa R. Effect of limestone dosages on some properties of geopolymer from thermally activated halloysite. Constr Build Mater. 2019;217:28–35. https://doi.org/10.1016/j.conbuildmat.2019.05.058.
58. Rees CA, Provis JL, Lukey GC, van Deventer JSJ. Attenuated total reflectance Fourier transform infrared analysis of fly ash geopolymer gel ageing. Langmuir. 2007;23(15):8170–9. https://doi.org/10.1021/la700713g.
59. Kamseu E, Kaze CR, Fekoua JNN, Melo UC, Rossignol S, Leonelli C. Ferrisilicates formation during the geopolymerization of natural Fe-rich aluminosilicate precursors. Mater Chem Phys. 2020;240: 122062. https://doi.org/10.1016/j.matchemphys.2019.122062.
60. Kaze CR, Yankwa JN, Nana A, Tchakoute HK, Kamseu E, Melo UC, Rahier H. Effect of silicate modulus on the setting, mechanical strength and microstructure of iron-rich aluminosilicate (laterite) based-geopolymer cured at room temperature. Ceram Int. 2018;44(17):21442–50. https://doi.org/10.1016/j.ceramint.2018.08.205.
61. Xu H, Gong W, Syltebo L, Izzo K, Lutze W, Pegg IL. Effect of blast furnace slag grades on fly ash based geopolymer waste forms. Fuel. 2014;133:332–40. https://doi.org/10.1016/j.fuel.2014.05.018.
62. Kamseu E, Leonelli C, Perera DS, Melo UC, Lemougna PN. Investigation of volcanic ash based geopolymers as potential building materials. Int Ceram Rev. 2009;58(2–3):136–40.
63. Nana A, Ngouné J, Kaze RC, Boubakar L, Tchounang SK, Tchakouté HK, Kamseu E, Leonelli C. Room-temperature alkaline activation of feldspathic solid solutions: development of high strength geopolymers. Constr Build Mater. 2019;195:258–68. https://doi.org/10.1016/j.conbuildmat.2018.11.068.
64. Moudio AMN, Tchakoute HK, Ngnintedem DLV, Andreola F, Kamseu E, Nanseu-Njiki CP, Leonelli C, Rüscher CH. Influence of the synthetic calcium aluminate hydrate and the mixture of calcium aluminate and silicate hydrates on the compressive strengths and the microstructure of metakaolin-based geopolymer cements Mater. Chem Phys. 2021;264: 124459. https://doi.org/10.1016/j.matchemphys.2021.124459.
65. Huo Z, Xu X, Lü Z, Song J, He M, Li Z, Wang Q, Yan L. Synthesis of zeolite NaP with controllable morphologies. Micropor Mesopor Mater. 2012;158:137–40. https://doi.org/10.1016/J.MICROMESO.2012.03.026.
66. Tchakouté HK, Rüscher CH, Kong S, Kamseu E, Leonelli C. Geopolymer binders from metakaolin using sodium waterglass from waste glass and rice husk ash as alternative activators: a

comparative study. Constr Build Mater. 2016;114:276–89. https://doi.org/10.1016/j.conbuildmat.2016.03.184.
67. Wan Q, Rao F, Song S, García RE, Estrella RM, Patiño CL, Zhang Y. Geopolymerization reaction, microstructure and simulation of metakaolin based geopolymers at extended Si/Al ratios. Cem Concr Compos. 2017;79:45–52. https://doi.org/10.1016/j.cemconcomp.2017.01.014.
68. Wan-En O, Yun-Ming L, Cheng-Yong H, Abdullah MM, Li L, Ho LN, Loong FK, Shee-Ween O, Hui-Teng N, Yong-Sing N, Jaya NA. Comparative mechanical and microstructural properties of high calcium fly ash one-part geopolymers activated with Na_2SiO_3-anhydrous and $NaAlO_2$. J Mater Res Technol. 2021;15:3850–66. https://doi.org/10.1016/j.jmrt.2021.10.018.
69. Ismail I, Bernal SA, Provis JL, San Nicolas R, Hamdan S, van Deventer JSJ. Modification of phase evolution in alkali-activated blast furnace slag by the incorporation of fly ash. Cement Concr Compos. 2014;45:125–35. https://doi.org/10.1016/j.cemconcomp.2013.09.006.